Optics Communications 283 (2010) 2596–2602

Contents lists available at ScienceDirect

Optics Communications

journal homepage: www.elsevier.com/locate/optcom

Beam properties of injection profiled quantum dot lasers

Vinod Vukkalam [a], John Houlihan [a,b,*]

[a] Department of Computing, Maths and Physics, Waterford Institute of Technology, Waterford, Ireland
[b] Tyndall National Institute, Lee Maltings, Cork, Ireland

ARTICLE INFO

Article history:
Received 7 December 2009
Received in revised form 10 February 2010
Accepted 14 February 2010

ABSTRACT

The impact of injection current profiling on the spatial mode structure of quantum dot semiconductor lasers is investigated. Numerical simulations based on a spatial extension of a simple rate equation model for quantum dot devices reveal the role of non-resonant carries in the appearance of strong dips in the optical field of the device. Symmetry breaking may also occur whereby the position of the dip shifts from the centre of the injection region.

© 2010 Elsevier B.V. All rights reserved.

1. Introduction

In the development of semiconductor laser (SL) technology over recent decades, researchers have made significant progress by inventing schemes to provide ever greater carrier and photon control. A recent example of this is the development of quantum dot (QD) photonic materials, sometimes called artificial atoms as the aim is to provide three dimensional confinement of injected carriers [1]. When applied to SLs, significant improvements have been achieved due to the combination of atomic and solid state characteristics of QD materials including lower, temperature insensitive threshold currents [1] and a lower sensitivity to optical feedback [2]. In addition, passively modelocked monolithic devices have demonstrated reduced timing jitter [3] and broad area devices have demonstrated reduced filamentation and improved M^2 characteristics [4–6]. QD materials also find applications in quantum information applications where their atomic character enables non-classical light sources to be realized [7]. Besides their technological importance, the use QD SLs has proved fruitful in the study of a variety of dynamical phenomena related to excitability in injection locked SLs [8]. In general, the enhanced performance of QD SLs in such technological applications and scientific studies has been attributed to their reduced phase amplitude coupling and increased relaxation oscillation damping, both of which delay the onset of dynamical instabilities in the system under consideration [9,10].

In this paper, we consider the application of QD materials to broad area injection profiled SLs. In addition to their technological interest as high brightness emitters, such devices have been important tools in the general study of transverse structures in spatially extended non-linear systems [11]. Injection profiling has previously been demonstrated as an extremely simple method to increase the stability range of broad area quantum well based SLs [12]. In such devices, the onset of spatio-temporal instability is delayed due to the existence of a strong, carrier induced anti-guide resulting from the combination of a smooth profiled injection and a significant phase amplitude coupling [13]. In this situation, the optical field follows the injection profile in the near field of the laser and displays off-axis emission in the far field (as originally predicted by Petermann [27]). To date, injection profiling has been implemented in quantum well SLs using contact patterning [12] and the inclusion of a spreading layer [23]. Both techniques provide coherent output to high pump levels in the pulsed regime, however, operation in the continuous thermal regime results in the cancellation of the stabilizing anti-guide by an injection induced thermal guide and typically, unstable filamentary operation results [14].

Recently, we studied the effect of injection profiling on QD based SLs experimentally as a function of device length in a current spreading layer structure [15]. As in the quantum well case, the carrier induced anti-guide stabilizes the optical field of the device and results in coherent off-axis emission in the far field. However, a notable difference appears in the near field, where a strong dip in intensity occurs at the peak of the injection profile (see Fig. 1). This dip persists to high injection levels until it disappears with the onset of filamentary dynamics. This near field feature is unique to QD based devices and does not occur in QW based structures. In this paper, we employ a rate equation description of the QD SL to explain the origin of this localised feature.

2. Quantum dot model

There exist several approaches to modeling spatially extended QD SLs. These vary in complexity, ranging from a full

* Corresponding author. Address: Department of Computing, Maths and Physics, Waterford Institute of Technology, Waterford, Ireland. Tel.: +353 21 490 4852; fax: +353 21 427 6949.
E-mail address: jhoulihan@wit.ie (J. Houlihan).

0030-4018/$ - see front matter © 2010 Elsevier B.V. All rights reserved.
doi:10.1016/j.optcom.2010.02.036

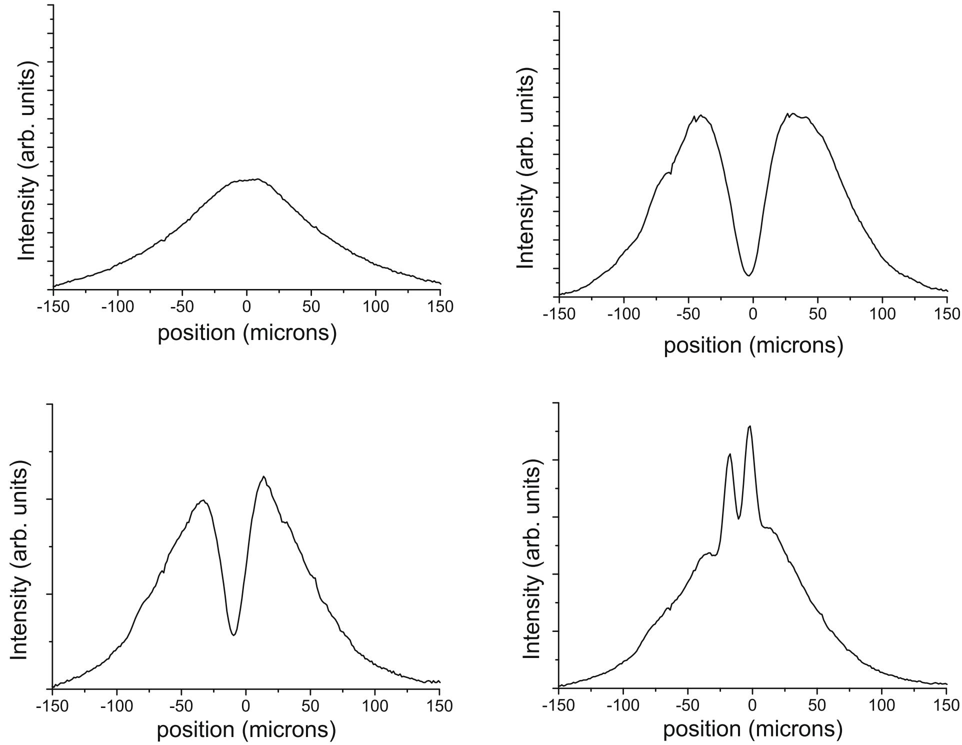

Fig. 1. Experimentally obtained near field intensity distributions for various currents in an injection profiled quantum dot laser. Note the appearance of a strong dip in the centre of the device which coincides with stable operation (top left – 120 mA below threshold, top right – 1.2 A coherent output, bottom left – 2 A coherent output, and bottom right – 2.5 A unstable output.

spatio-temporal multi-mode Maxwell–Bloch approach where the material parameters are derived from microscopic calculations [16] to less complicated rate equation models [17,18]. It should be noted that calculations of the optical matrix elements in InAs QDs have shown a sensitive dependence on quantum dot size, shape and composition [19]. For simplicity, and to avoid the introduction of a large number of unknown parameters, we follow the rate equation approach to the modeling of QD carrier dynamics and consider direct injection of carriers into the wetting layer (WL) of the device, from where they can be captured into the dot. The capture rate of this process is strongly dependent on the occupancy of the dot as a result of Pauli blocking due to the limited number of states in the dot. Previous studies of injection profiling in QW devices demonstrated that longitudinal mode dynamics were largely unimportant [23] and we therefore consider spatial effects in one transverse dimension only. Furthermore, the model neglects carrier transport within the active region. A similar approximation was used in the analysis of injection profiled QW devices [13] and indeed, such transport effects are expected to be reduced when going from QW to QD materials due to the increased spatial confinement of the carriers [6]. The corresponding equations for the occupancy of the QD (ρ) and WL carrier density per dot (N) read:

$$\frac{\partial \rho}{\partial t} = -\gamma_d \rho + CN(1-\rho) - v_g \sigma (2\rho - 1)|E|^2 \quad (1)$$

$$\frac{\partial N}{\partial t} = \frac{J(x)}{q} - \gamma_n N - 2CN(1-\rho) \quad (2)$$

where γ_n, γ_d are the non-radiative decay rates for carriers in the WL and dot, respectively, C is the capture rate from wetting layer into an empty dot, $J(x)$ is the spatially varying injection current per dot (a Lorentzian shape is used throughout), v_g is the group velocity, σ is the cross section of interaction of the carriers in a dot with the electric field, q is elementary charge, E is the complex amplitude of the electric field in the cavity, normalised to the photon density $S = |E|^2$.

When the dot population is coupled to the electric field within the cavity, the resulting gain is $g_0(2\rho - 1)$. The refractive index can have contributions from both the dot and wetting layer populations, as previously outlined both theoretically and experimentally and so the spatially varying electric field is governed by,

$$\frac{\partial E}{\partial t} = -\frac{1}{2}\gamma_s E + \frac{1}{2}(1 + i\alpha_d) v_g g_0 (2\rho - 1)E + i\alpha_{nr} v_g g_0 NE + iD_e \frac{\partial^2 E}{\partial x^2} \quad (3)$$

where γ_s is the photon decay rate in the cavity, g_0 the differential gain, α_d and α_{nr} describe the change of refractive index with change of dot carrier population and with non-resonant population, respectively, and $D_e = \frac{c}{2k_0\eta^2}$ refers to the diffraction coefficient of light (where k_0 represents the wavenumber in the vacuum, c is the velocity of light and η is the effective refractive index). In typical self-assembled QD materials, carriers can be present in the wetting layer or in various excited states of the dot. In addition, variation in the

Table 1
Parameters used in the model corresponding to a 60% contribution from non-resonant carriers to α_{th}.

$\gamma_n = \gamma_d = 10^{-3}$ (ps)$^{-1}$		
$\gamma_s = 0.3$ (ps)$^{-1}$		
$v_g = 167 \times 10^6$ m/s		
$C = 10^{-1}$ (ps)$^{-1}$		
$\lambda = 1310$ nm		
$\eta = 3.5$		
For $\rho_{th} = 0.9$	$g_0 = 22.5$ (cm)$^{-1}$	$\sigma = 1.88 \times 10^{-7}$ (μm)^2
$\alpha_{th} = 3$	$\alpha_d = 1.2$	$\alpha_{nr} = 0.45$
For $\rho_{th} = 0.6$	$g_0 = 90$ (cm)$^{-1}$	$\sigma = 7.5 \times 10^{-7}$ (μm)^2
$\alpha_{th} = 1.5$	$\alpha_d = 0.6$	$\alpha_{nr} = 14.4$

size of the dot due to the nature of self-assembly growth leads to an in inhomogeneous broadening of each of the dot's energy levels. Introducing additional non-resonant levels and carrier transport between different sized dots involves a substantial increase in complexity and the introduction of many additional parameters that are not well known. To avoid such issues, we confine the model to a single dot state ρ, and a single non-resonant population N.

As our QD laser model is essentially a spatial extension of the rate equation model investigated by Melnik et al. [20], we will follow their parameter values here unless otherwise mentioned. In that paper, it was demonstrated that the unique carrier dynamics of QD materials could lead to different values for the linewidth enhancement factor (α) when measured using different techniques, particularly in the case where the dot's population becomes saturated. To investigate the reported behaviour of current profiled QD lasers [15] we will also contrast the saturated and unsaturated cases, which experimentally correspond to short and long devices, respectively. In order to choose values for α_d and α_{nr}, we note experimental evidence that α at threshold (α_{th}) ranges from 1.5 to 3 when going from long to short devices [21]. In addition, the corresponding free-carrier contribution to α ranges from 40–60% [22], and also depends on length. From [20], the parameters α_d and α_{nr} are related to α_{th} according to,

$$\alpha_{th} = \alpha_d + \alpha_{nr}\left(\frac{\delta N}{\delta \rho}\right) \quad \text{and} \quad \frac{\delta N}{\delta \rho} = \frac{\gamma_d}{(C(1-\rho_{th})^2)} \tag{4}$$

where ρ_{th} is the dot population at laser threshold. The corresponding list of parameters is given in Table 1 for both saturated and unsaturated operating conditions, and correspond to a 60% contribution from non-resonant carriers to α_{th}.

3. Narrow injection profiles

Before investigating the wide injection profiles which occurred in the experimental data in Fig. 1, we examined a narrower 35 μm injection width for both saturated ($\rho_{th} = 0.9$) and unsaturated ($\rho_{th} = 0.6$) dots. This examination is useful to compare the results

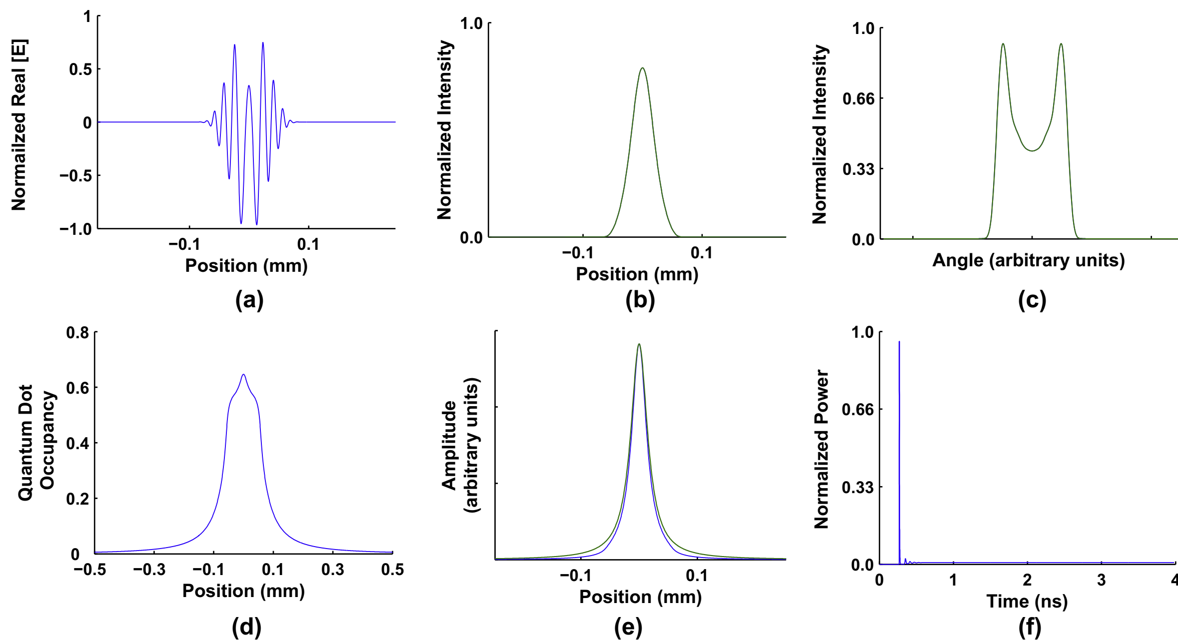

Fig. 2. Simulated beam properties for a 35 μm wide Lorentzian injection profile in the unsaturated regime ($\rho_{ss} = 0.6$) at $6J_{th}$. (a) Instantaneous near field electric field; (b) instantaneous (blue) and time averaged (green) near field intensities; (c) instantaneous (blue) and time averaged (green) far field intensities; (d) QD occupancy; (e) normalised injection profile (green) and non-resonant carrier profile (blue); and (f) normalised output power as a function of time. (For interpretation of the references to colour in this figure legend, the reader is referred to the web version of this article.)

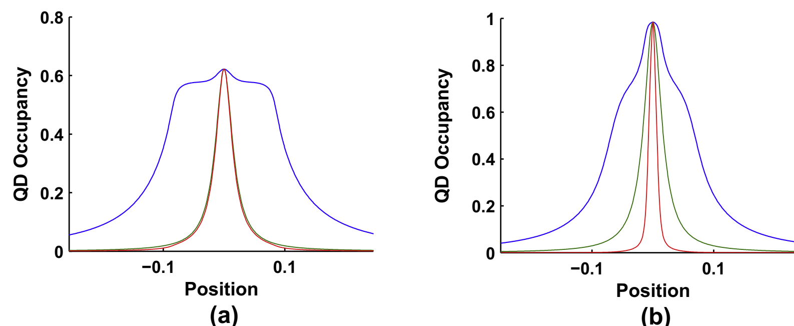

Fig. 3. Injection profile (green) and non-resonant carrier profile (red), both normalised to QD occupancy (blue), compared for (a) unsaturated and (b) saturated regimes. Note the significant narrowing of the non-resonant carrier profile in the saturated case. Injection levels were $5J_{th}$ for unsaturated case and $8J_{th}$ for saturated case. (For interpretation of the references to colour in this figure legend, the reader is referred to the web version of this article.)

of the QD simulation to previous studies of injection profiling in QW devices [13]. A snapshot of the output of the simulation, once it has reached steady state, is shown in Fig. 2 for $\rho_{th} = 0.6, J = 6J_{th}$, i.e. the unsaturated case. The behaviour is very similar to that previously reported for the QW case, i.e. the near field intensity profile follows the pump profile and consists of two spatially separated counter-propagating traveling waves resulting in distinct, off-axis emission in the far field, stabilized by a carrier induced anti-guide [23]. This behaviour persists to $\sim 8J_{th}$ before the onset of filamentary dynamics. Very similar behaviour is observed for the case where the dot is saturated ($\rho_{th} = 0.9$), however, the instability level in this case increases to $\sim 24J_{th}$.

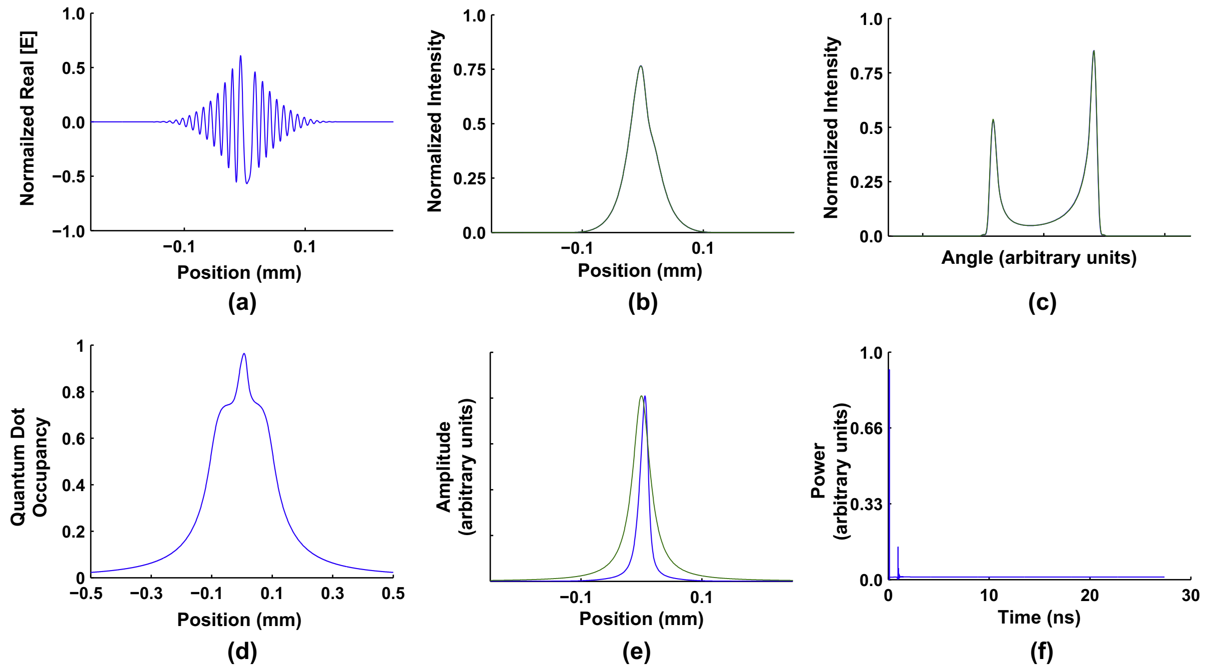

Fig. 4. Simulated beam properties for a 35 μm wide Lorentzian injection profile in the saturated regime ($\rho_{ss} = 0.9$) at $18J_{th}$. (a) Instantaneous near field electric field; (b) instantaneous (blue) and time averaged (green) near field intensities; (c) instantaneous (blue) and time averaged (green) far field intensities; (d) QD occupancy; (e) normalised injection profile (green) and non-resonant carrier profile (blue); and (f) normalised output power as a function of time. Note asymmetric behaviour in near and far fields, and carrier densities. (For interpretation of the references to colour in this figure legend, the reader is referred to the web version of this article.)

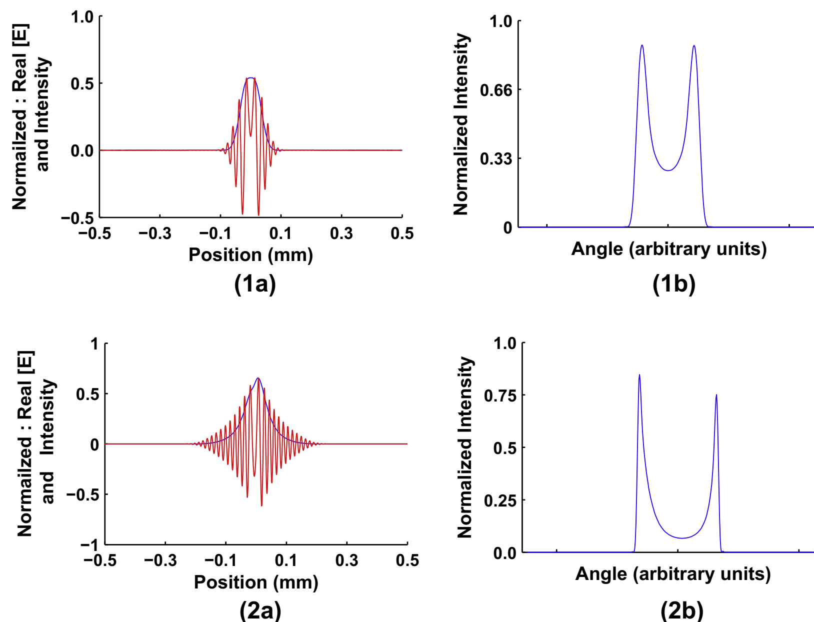

Fig. 5. Simulated beam properties for a 70 μm wide Lorentzian injection profile in the saturated regime ($\rho_{ss} = 0.9$) at low ($3J_{th}$) and high ($16J_{th}$) injection levels. 1(a) and 2(a) contain near field electric field (red) and near field intensity (blue) for low (1(a)) and high (2(a)) injection levels. 1(b) and 2(b) contain the far field intensities for low and high injection, respectively. Note the asymmetric behaviour at high injection. (For interpretation of the references to colour in this figure legend, the reader is referred to the web version of this article.)

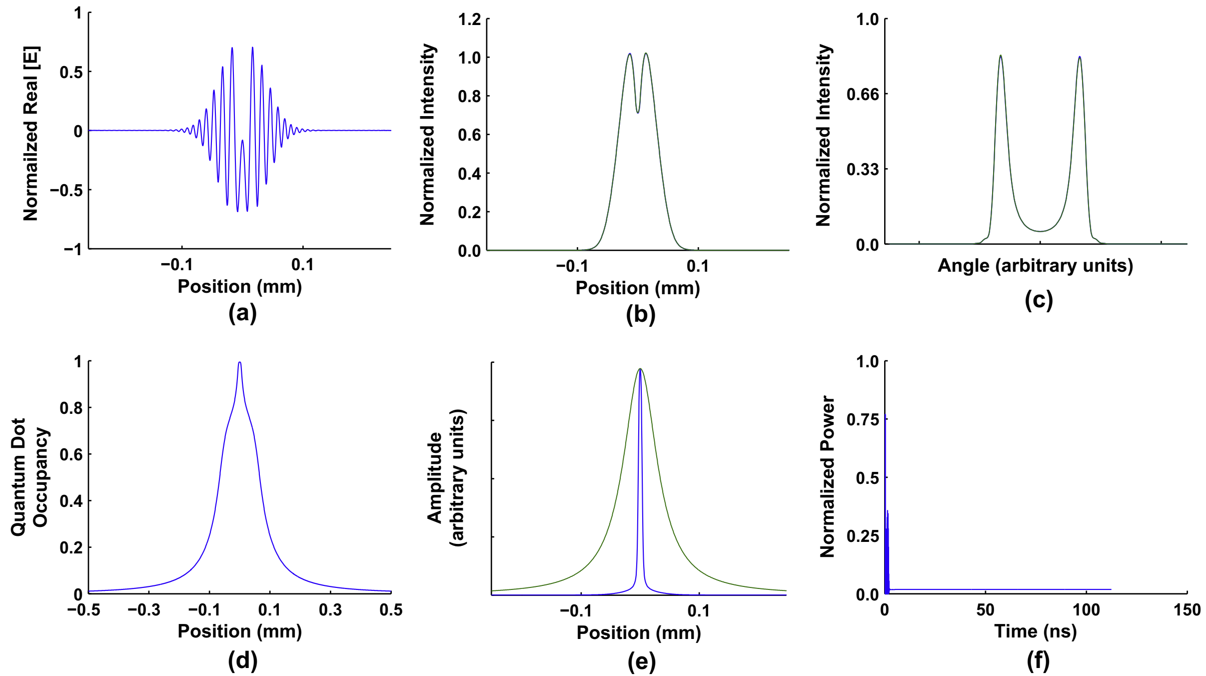

Fig. 6. Simulated beam properties for a 70 μm wide Lorentzian injection profile in the saturated regime at increased phase amplitude coupling ($\alpha_{th} = 9$, injection level $2J_{th}$). (a) Instantaneous near field electric field; (b) instantaneous (blue) and time averaged (green) near field intensities; (c) instantaneous (blue) and time averaged (green) far field intensities; (d) QD occupancy; (e) normalised injection profile (green) and non-resonant carrier profile (blue); and (f) normalised output power as a function of time, Note presence of a strong dip on the centre of the near field, similar to the experimental dip seen in Fig. 1. (For interpretation of the references to colour in this figure legend, the reader is referred to the web version of this article.)

It is worthwhile highlighting that, in the saturated case, the steady state non-resonant carrier profiles are substantially narrower than the injection profile. This is not the case for the unsaturated dots and suggests that the reduced rate of carrier capture in the saturated case (due to Pauli blocking), results in a build-up of non-resonant carriers in the centre of the device, thereby narrowing the non-resonant carrier profile (see Fig. 3 for comparison). The impact of such a buildup can be seen in Fig. 4 where the symmetric solution has become unstable at high injection due to the high level of non-resonant carriers and a stable asymmetric solution results where the source of traveling waves has moved to one side of the injection profile. A similar symmetry breaking was observed in [11] for QW injection profiled lasers with a broad flat central pump region. In that case, the source of the traveling waves in the near field moves from the centre to one of the edges of the injection profile.

4. Wide injection profiles

The next step is to simulate the wider injection profiles which occurred in the experiment. For the parameters outlined in Table 1 and an injection width of 70 μm the behaviour was very similar to that outlined for the narrower injection profiles for both saturated and unsaturated dot cases. An example of this for the saturated case is shown in Fig. 5 for low and high injection and displays very similar features to the narrower case, i.e. a single lobed near field and double lobed far field. Again, the steady state non-resonant carrier profiles are substantially narrower than the injection profile (in contrast to the unsaturated situation) and symmetry breaking occurs in the near and far fields in a similar manner to the narrower pump case.

A significant impact of the carrier buildup can be seen for increased values of the threshold phase amplitude coupling, α_{th}. If the value is increased from 3 to 9, interesting features emerge. It should be noted that such high values for the phase amplitude coupling have been reported in the saturated regime, where two state lasing occurs [24]. As shown in the high injection case in Fig. 6, a stable solution can occur whereby a large dip in intensity appears near the centre of the near field. This coincides with a further narrowing of the non-resonant carrier profile. The appearance of such a dip in the near field intensity profile is very similar to that observed experimentally (see Fig. 1). In the simulation, such dips gradually emerge in the near field as injection is increased due to the increasing non-resonant carrier density and high level of associated anti-guiding due to α_{nr}. Interestingly, a very similar behaviour occurs in the experiment as shown in Fig. 7, wherein the level of the dip increased with injection. Also, some asymmetry appears in the experiment at increased injection (Fig. 1, bottom left panel), such asymmetry also occurs in the simulation at increased

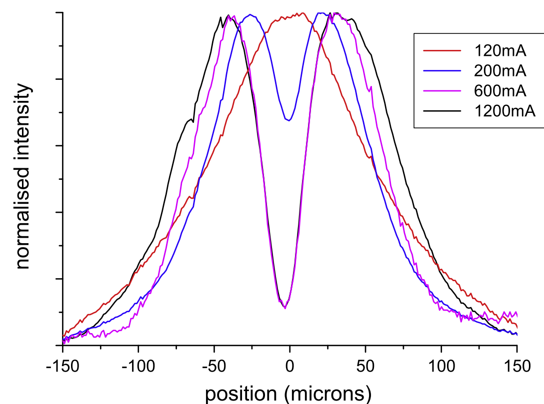

Fig. 7. Experimental normalised time averaged near field intensities at different injection levels. Note the gradual emergence of the central dip as the injection level increases to 600 mA. Similar behaviour is seen in the simulation.

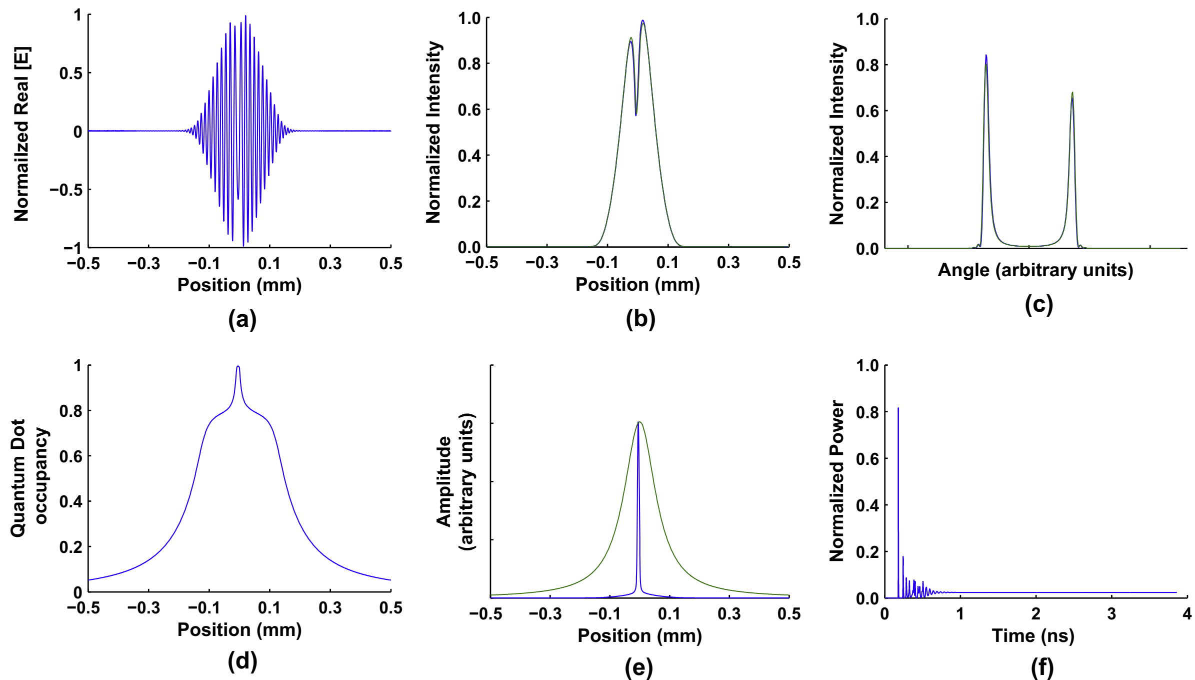

Fig. 8. Simulated beam properties for a 130 μm wide Lorentzian injection profile in the saturated regime at increased phase amplitude coupling ($\alpha_{th} = 9$, injection level $3J_{th}$). (a) Instantaneous near field electric field; (b) instantaneous (blue) and time averaged (green) near field intensities; (c) instantaneous (blue) and time averaged (green) far field intensities; (d) QD occupancy; (e) normalised injection profile (green) and non-resonant carrier profile (blue); and (f) normalised output power as a function of time, Note presence of a strong dip on the centre of the near field, together with asymmetric field and carrier profiles. (For interpretation of the references to colour in this figure legend, the reader is referred to the web version of this article.)

injection levels. It is important to note that, in the simulation, such a dip does not occur for the unsaturated case at the same level of phase amplitude coupling, probably due to the lack of a narrow non-resonant carrier induced anti-guide.

For even wider injection profiles, up to 130 μm, the behaviour seen for the 70 μm injection case continues. In the unsaturated case, the symmetric traveling wave solution appears. In the saturated case, the stable solution is typically asymmetric as before and includes a strong dip in intensity due to non-resonant carrier induced anti-guiding, see Fig. 8 for an example of this behaviour.

5. Discussion

In the previous sections, the beam properties of injection profiled QD SL were analysed. The spatial extension of a simple QD model based on separate carrier populations for saturable resonant QD states and non-resonant states was presented. Such a model neglects the possibility of lasing from excited dot states [25] and different relaxation timescales for electrons and holes [26], however, despite these approximations, the model qualitatively provides insights on observed phenomena unique to QD devices.

Experimentally, a strong dip appears in the near field of the wide injection profiled devices. In the numerical simulations, a similar dip also appears when the injection profile width increases beyond ∼70 μm for high phase amplitude coupling when the resonant states are close to saturation. This dip emerges gradually as the injection increases, a trend also seen in the experiment. From the numerical simulations, this dip can be attributed to increased anti-guiding in the region of the dip, due to non-resonant carrier buildup and a subsequent narrowing of the non-resonant carrier profile. In addition, spontaneous symmetry breaking was observed in the simulation, whereby the position of the source of the transverse traveling waves in the near field shifts from the centre of the injection region. Some preliminary evidence for this behaviour was presented.

To investigate the sensitivity of these novel features to variation in the parameter values, the relative contribution of non-resonant carriers to the overall phase amplitude couple was varied. As this contribution is reduced from 60% to 50%, no marked difference in the output beam properties are observed. However, on reduction of the non-resonant contribution to 40% the characteristic dip in the near field is significantly reduced. In addition, the range of profile widths and pump levels where stable, non-filamentary output occurs is also reduced. In the future, more detailed experiments and simulations are planned to further investigate such issues and additional factors unique to QDs such as the separate roles of excited dot and quantum well wetting layer states, and the different recombination times of electrons and holes due to the difference in effective mass [25].

6. Conclusions

The unique carrier dynamics of QD devices results in novel features in the optical fields of injection profiled SLs. In particular, a strong dip in the intensity distribution across the device is attributed to increased localised anti-guiding due to non-resonant carrier buildup when the resonant population is close to saturation. In addition, symmetry breaking may also occur in the saturated dot case where the source of transverse traveling wave shifts from the centre of the device.

Acknowledgements

The authors would like to acknowledge financial support from the Institute of Technology Ireland's Strand I program and access to QD structures under the Tyndall National Access Program (NAP).

References

[1] D. Bimberg, M. Grundmann, N.N. Ledentsov, Quantum Dot Hetero-Structures, Wiley, New York, 1999.
[2] D. O'Brien, S.P. Hegarty, G. Huyet, J.G. McInerney, T. Kettler, M. Laemmlin, D. Bimberg, V.M. Ustinov, A.E. Zhukov, S.S. Mikhrin, A.R. Kovsh, IEE Electron. Lett. 39 (2003) 1819.
[3] M.T. Todaro, J.P. Tourrenc, S.P. Hegarty, C. Kelleher, B. Corbett, G. Huyet, J.G. McInerney, Opt. Lett. 31 (2006) 3107.
[4] P.M. Smowton, E.J. Pearce, H.C. Schneider, W.W. Chow, M. Hopkinson, Appl. Phys. Lett. 81 (17) (2002) 3251.
[5] S. Fathpour, P. Bhattacharya, S. Pradhan, S. Ghosh, IEE Electron. Lett. 39 (20) (2003) 1443.
[6] Ch. Ribbat, R.L. Sellin, I. Kaiander, F. Hopfer, N.N. Ledentsov, D. Bimberg, A.R. Kovsh, V.M. Ustinov, A.E. Zhukov, M.V. Maximov, Appl. Phys. Lett. 82 (6) (2003) 952.
[7] P. Michler, A. Kiraz, C. Becher, W.V. Schoenfeld, P.M. Petroff, Lidong Zhang, E. Hu, A. Imamoglu, Science 290 (5500) (2000) 2282.
[8] D. Goulding, S.P. Hegarty, O. Rasskazov, S. Melnik, M. Hartnett, G. Greene, J.G. McInerney, D. Rachinskii, G. Huyet, Phys. Rev. Lett. 98 (2007) 153903.
[9] M. Kuntz, N.N. Ledentsov, D. Bimberg, A.R. Kovsh, V.M. Ustinov, A.E. Zhukov, Y.M. Shernyakov, Appl. Phys. Lett. 81 (2002) 3846.
[10] D. O'Brien, S.P. Hegarty, G. Huyet, A.V. Uskov, Opt. Lett. 29 (2004) 10.
[11] E. O'Neill, J. Houlihan, J.G. McInerney, G. Huyet, Phys. Rev. Lett. 94 (2005) 143901.
[12] C. Lindsey, P. Derry, A. Yariv, Electron. Lett. 21 (1985) 671.
[13] V. Voignier, J. Houlihan, J.R. O'Callaghan, C. Saillot, G. Huyet, Phys. Rev. A 65 (2002) 053807.
[14] J.R. O'Callaghan, J. Houlihan, V. Voignier, G.H. Wu, E. O'Neill, J.G. McInerney, G. Huyet, IEEE J. Quant. Electron. 40 (1) (2002) 1.
[15] J. Houlihan, C. Kelleher, Opt. Commun. 281 (5) (2008) 1156.
[16] E. Gehrig, O. Hess, Phys. Rev. A 65 (2002) 033804.
[17] A.V. Uskov, E.P. O'Reilly, R.J. Manning, R.P. Webb, D. Cotter, M. Laemmlin, N.N. Ledentsov, D. Bimberg, IEEE Photon. Technol. Lett. 16 (2004) 1265.
[18] M. Sugawara, K. Mukai, H. Shoji, Appl. Phys. Lett. 71 (1997) 2791.
[19] A.D. Andreev, E.P. O'Reilly, Appl. Phys. Lett. 87 (2005) 213106.
[20] S. Melnik, G. Huyet, A.V. Uskov, Opt. Exp. 14 (7) (2006) 29650.
[21] J. Muszalski, J. Houlihan, G. Huyet, B. Corbett, Electron. Lett. 40 (7) (2004) 428.
[22] S.P. Hegarty, B. Corbett, J.G. McInerney, G. Huyet, Electron. Lett. 41 (2005).
[23] J. Houlihan, J.R. O'Callaghan, V. Voignier, G. Huyet, J.G. McInerney, B. Corbett, Opt. Lett. 26 (20) (2001) 1556.
[24] B. Dagens, A. Markus, J.X. Chen, J.-G. Provost, D. Make, O. Le Gouezigou, J. Landreau, A. Fiore, B. Thedrez, Electron. Lett. 41 (6) (2005) 323.
[25] E.A. Viktorov, P. Mandel, Y. Tanguy, J. Houlihan, G. Huyet, Appl. Phys. Lett. 87 (2005) 053113.
[26] I. O'Driscoll, T. Piwonski, C.-F. Schleussner, J. Houlihan, G. Huyet, R.J. Manning, Appl. Phys. Lett. 91 (2007) 071111.
[27] K. Petermann, Opt. Quant. Electron. 13 (1981) 323.